Available online at www.sciencedirect.com

ScienceDirect

Advances in Space Research 56 (2015) 47–56

ADVANCES IN SPACE RESEARCH (a COSPAR publication)

www.elsevier.com/locate/asr

Effects of plasma drag on low Earth orbiting satellites due to solar forcing induced perturbations and heating ☆

Victor U.J. Nwankwo [a,*], Sandip K. Chakrabarti [a,b], Robert S. Weigel [c]

[a] S. N. Bose National Centre For Basic Sciences, Kolkata 700098, India
[b] Indian Centre for Space Physics, Kolkata 700084, India
[c] George Mason University, 4400 University Drive, Fairfax, VA 22030, USA

Received 16 September 2014; received in revised form 14 January 2015; accepted 30 March 2015
Available online 9 April 2015

Abstract

The upper atmosphere changes significantly in temperature, density and composition as a result of solar cycle variations, which causes severe storms and flares, and increases in the amount of absorbed solar radiation from solar energetic events. Satellite orbits are consequently affected by this process, especially those in low Earth orbit (LEO). In this paper, we present a model of atmospheric drag effects on the trajectory of two hypothetical LEO satellites of different ballistic coefficients, initially injected at $h = 450$ km. We investigate long-term trends of atmospheric drag on LEO satellites due to solar forcing induced atmospheric perturbations and heating at different phases of the solar cycle, and during short intervals of strong geomagnetic disturbances or magnetic storms. We show dependence of orbital decay on the severity of both solar cycle and phase and the extent of geomagnetic perturbations. The result of the model compares well with observed decay profile of some existing LEO satellites and provide a justification of the theoretical considerations used here.

Keywords: Ballistic coefficient; LEO satellite trajectory; Plasma drag; Solar cycle variations; Solar energetic events

1. Introduction

Once launched, the optimum performance and survival of a satellite depend on its ability to weather both gravitational and non-gravitational perturbing forces including atmospheric drag, especially for satellites at low Earth orbit. Atmospheric drag on LEO satellites (corresponding to altitudes of < 800 km) can cause untimely re-entry of satellites, difficulty in identifying and tracking of satellites and other space objects, manuvering and prediction of lifetime and actual re-entry (Klinkrad, 1996; Mark et al., 2005; Doornbos and Klinkrad, 2006; Xu et al., 2011; Walterscheid, 1989; Nwankwo and Chakrabarti, 2014, 2015). Accelerated orbit decay due to atmospheric drag on low Earth orbiting satellites is mainly due to solar forcing induced variations in thermospheric density profile. There have been studies that investigated the response of thermospheric density and/or satellites orbit to variations in solar forcing due to solar activity using one or combination of several methods such as simulations, satellite drag data, on-orbit mass spectrometers, accelerometers, sounding rockets and ground-based incoherent scatter radars (Klinkrad, 1996; Xu et al., 2011; Burns et al., 2012; Leonard et al., 2012; Kutiev et al., 2013; Lei et al., 2013; Chen et al., 2012; Kwak et al., 2011; Solomon et al., 2012; Liu et al., 2012; Lei et al., 2008; Sutton et al., 2005; Deng et al., 2012; Walterscheid, 1989; Weigel et al., 2004; Weigel, 2010; Nwankwo and Chakrabarti, 2014, 2015). It is known that density of the thermosphere and the vertical

☆ Presented in COSPAR 2014, Moscow, Russia.

* Corresponding author at: S. N. Bose National Centre For Basic Sciences, Kolkata, JD Block, Salt Lake, Kolkata 700098, India. Tel.: +91 33 2335 5706; fax: +91 33 2335 9176.
E-mail addresses: victorujn@bose.res.in (V.U.J. Nwankwo), chakraba@bose.res.in (S.K. Chakrabarti), rweigel@gmu.edu (R.S. Weigel).

http://dx.doi.org/10.1016/j.asr.2015.03.044
0273-1177/

extent of the upper atmosphere varies on time scales of solar flare event (few hours), geomagnetic storms (1–3 days) and the solar cycle (~ 11 years) (Alfonsi et al., 2008; Bounsanto, 1999; Kutiev et al., 2013). There is a significant heating and consequent expansion of the upper atmosphere during solar and geomagnetic activities. Studies have shown that solar EUV and thermospheric temperature could increase by a factor of two (or more), and thermospheric density by a factor of up to ten from solar minimum to solar maximum (Emmert and Picone, 2010; Walterscheid, 1989). The contribution to upper atmospheric heating by solar EUV radiation is larger than that associated with geomagnetic current enhancement during time interval of enhanced geomagnetic activity. However, geomagnetic field induced Joule heating becomes important during short-term strong geomagnetic perturbations and can increase by up to 134% when the Kp index increases from 1 to 6 or Ap index from 4 to 80 (Rhoden et al., 2000; Kim et al., 2006; Chen et al., 2012; Kutiev et al., 2013).

Solar energetic events that cause atmospheric heating include solar wind streams, coronal mass ejections (CMEs), solar flares and corotating interaction regions (CIRs). When a solar wind high-speed stream (HSS) emanates from the sun, it interacts with preceding low-speed solar winds and form a corotating interactive region (CIR). The interface between low and high speed solar plasma (CIR) interacts with the Earth's magnetosphere and produces geomagnetic disturbances and storms (Borovsky and Denton, 2006; Burns et al., 2012; Gosling and Pizzo, 1999; Kutiev et al., 2013; Tsurutani et al., 2006). There are many studies which investigated the effects of CIRs or solar wind conditions on the thermosphere and satellite orbits (Burns et al., 2012; Solomon et al., 2012; Liu et al., 2012; Lei et al., 2008; Borovsky and Denton, 2006). CIRs and HSSs are known to be the dominant drivers of storm induced atmospheric perturbations during the declining phase of the solar cycle and are, therefore important to thermospheric density and satellite orbital variations during this phase of the cycle (Burns et al., 2012; Chen et al., 2012; Nwankwo and Chakrabarti, 2014). CMEs and solar flares are sporadic events and are known to vary with phase of a solar 11-year cycle. They are more frequent and intense during a solar maximum (Richardson et al., 2001; Gopalswamy, 2009). Thermal tides propagating upwards from the lower atmosphere can also influence atmospheric density and satellite orbits (Forbes et al., 2009; Hagan and Forbes, 2002; Zhang et al., 2010; Oberheide et al., 2009; Leonard et al., 2012; Nwankwo and Chakrabarti, 2014). Thermospheric density also exhibits annual, semiannual and diurnal oscillations (Emmert and Picone, 2010; Doornbos, 2012).

Some insightful investigations on space weather effects on thermosphere density and satellite orbit includes that of Walterscheid (1989), Chen et al. (2012), Leonard et al. (2012), Lei et al. (2013) and others. Walterscheid (1989) studied effects of the solar cycle on upper atmosphere and their implications on satellite drag and pointed out that a typical satellite initially at a height of 500 km could have a lifetime of about 30 years under typical solar cycle minimum conditions and only about 3 years under the solar maximum conditions (Nwankwo and Chakrabarti, 2014). Chen et al. (2012) investigated and compared effects of CIR- and CME-induced geomagnetic activity on thermospheric densities and spacecraft orbits, and found that CME-induced storms (although of shorter duration) causes larger thermosphere density disturbances and a resultant larger orbital decay rates during its main phase than CIR storms, but the mean thermospheric density and satellite orbit decay during CIR storms could be much larger than those during the CME-induced storms in each case because of longer duration of CIR phase. Lei et al. (2013) also studied the impact of solar forcing on thermospheric densities and spacecraft orbits from CHAMP and GRACE satellite's data during the events (CMEs and CIR) of September 14–28 and November 19–22, 2003, and showed that variations of the satellite's semi-major axis was 243 m for CIR-induced perturbations during September 15–27, 2003 and about 130 m for CME-induced storm event during November 19–22, 2003. These studies only used the data (on-orbit mass spectrometers and accelerometers) on existing satellites (e.g. CHAMP and GRACE). In this study, we incorporate the NRLMSISE-00 empirical atmospheric model into our drag model to investigate short- and long-term trends of atmospheric drag effects on LEO satellite orbits due to atmospheric density perturbations and heating by solar energetic events at different phases of the solar cycle. This study is important for understanding how satellite orbits are affected during short- and long-term variations in solar and geomagnetic activity using a realistic atmospheric density and drag model. We are aware of the difficulties associated with exact determination of atmospheric density and orbital predictions at very low Earth orbits. Therefore, we ignore impacts of tidal effects at this stage.

2. Upper atmospheric density profile

An accurate prediction of a satellite's lifetime, re-entry or drag depends on good knowledge of atmospheric density profile, which is an important space environmental parameter for satellite operation in the near-Earth space (Kwak et al., 2011; Chen et al., 2012). Although this quantity is not precisely known at any given instant, many atmospheric models have been developed (and more are being developed) over the years with good approximation. However, despite the unprecedented improvements in modeling atmospheric density, concerns about the accuracy of the models remain, because the individual effects of various solar forcing mechanism, which causes fluctuations in neutral and ionized density are very difficult to estimate and/or model (also, see Kutiev et al. (2013), Storz et al. (2005)). Particularly important are the hysteresis effects where the effects of the same event may depend on the history of events which took place before it. Some

atmospheric models in use include that of Picone et al. (2002), Bruinsma et al. (2003), Bowman et al. (2008), Emmert and Picone, 2010, Liu et al. (2013) and others. In our work, atmospheric density profiles are obtained from the NRLMSISE-00 empirical atmospheric model. Details of the model can be found in Picone et al. (2002). In addition to other outputs, NRLMSISE-00 gives total atmospheric mass density as a function of time, location, solar and geomagnetic activity. The model has also been used in some other works, such as, Policastri and Simons (2003), Doornbos (2012) and Klenzing et al. (2013).

3. Procedure

In this work, we consider two hypothetical satellites (SAT-BCI and SAT-BCII) with different ballistic coefficients [BCI ($m_s = 250$ kg, $A_s = 0.25$ m^2, $C_d = 2.2$) and BCII ($m_s = 522$ kg, $A_s = 0.72$ m^2, $C_d = 2.2$)], initially injected at an altitude of 450 km. The ballistic and/or drag coefficient used in this study were explained in Nwankwo and Chakrabarti (2014). We compute atmospheric drag force on the satellites due to long-term solar and geomagnetic activity at different phases of the solar cycle, viz. 2000–2002 (to represent a typical solar peak activity during the last solar maximum), 2004–2006 (to represent a typical solar 'quiet' period during last solar minimum), and 2012–2014 (to represent the period around current solar maximum). We thus obtain an estimate of the mean annual decay rate of the satellites at different phases of the solar cycle (minimum and maximum). We also compute and investigate the drag effect for short-term strong geomagnetic disturbances and/or storms in three regimes, with and without control on the solar parameters, aimed at providing insight into how the model works. Solar radio flux (F10.7), geomagnetic Ap index and the moving average of F10.7 over three solar rotations (81 days) were used in the model (NRLMSISE-00) as inputs to obtain thermosphere density profile (NOAA-1). Solar radio flux (F10.7) indirectly estimates upper atmospheric heating from solar energetic particles and solar extreme ultra-violet (EUV). Planetary Ap (or Kp) index estimates additional Joule heating associated with geomagnetic activity (Pardini et al., 2004; IRS Radio, 1999; NOAA, 2006). The moving average of F10.7 flux over three or four solar rotations, denoted by $\bar{F}_{10.7}$ represents a slowly varying component of solar radiation (Doornbos, 2012; Nwankwo and Chakrabarti, 2014).

4. Computation of orbital decay due to plasma drag

The orbital decay due to atmospheric drag on SAT-BCI and SAT-BCII are computed from two sets of equations to study both short- and long-term effects of space environmental perturbations on the trajectory of the model satellites. A spherical polar co-ordinate system (r, θ, ϕ) was used, with origin at the center of the Earth. We assume that the satellite always remain in the same plane (i.e., $\theta =$ constant). The first set of the equations used consists of four coupled differential equations (Nwankwo and Chakrabarti, 2014, 2015):

$$\dot{v}_r = -\frac{GM_e}{r^2} + r\dot{\phi}^2 \tag{1}$$

$$\dot{r} = v_r \tag{2}$$

$$\ddot{\phi} = -\frac{1}{2} r\rho\dot{\phi}^2 \frac{A_s C_d}{m_s} \tag{3}$$

$$\dot{\phi} = v_\phi / r \tag{4}$$

where, v_r and v_ϕ are the radial and tangential velocity components, G is the gravitational constant, M_e is the mass of the Earth, r is the instantaneous radius of the orbit, ρ could be the atmospheric density, A_s is the omni-directional projected area of the satellite, m_s is the mass of the satellite, and C_d is the drag coefficient at an altitude of r.

The equations were solved to obtain instantaneous position and velocity of the satellite. Orbital decay due to atmospheric drag on the model satellites were computed under varying space weather conditions, while tracking their position and time by the azimuthal parameters $(\phi, \dot{\phi})$. Other integration (such as, $-\dot{\phi}r^2(A_sC_d/m_s)$) gave similar results (Chobotov, 2002). The second equation is a differential equation ($dr/dt = -\rho(A_sC_d/m_s)\sqrt{GMr}$), that describes changes in the mean radius of the satellite orbit per revolution (MRPR) (Xu et al., 2011; Chen et al., 2012; Wertz and Larson, 1999). Model results of orbital decay profile in the two set of equations (or methods) generally agree.

4.1. Modeling CIR-induced periodic changes in atmospheric density profile

The empirical atmospheric model used in this work is assumed to have a good representation of the background thermospheric density including storm induced fluctuations and a varying component due to solar rotation (introduced through the solar radio flux, geomagnetic Ap index and the $\bar{F}_{10.7}$). CIR-induced effects on thermospheric density is known to be dominant during the solar minimum and, therefore produces significant decay of satellite orbits at this phase of the solar cycle. Although the model to some extent includes CIR effects through the geomagnetic activity index input, its associated effects may be underestimated due to its high frequency (dominance) at this phase. Lindsay et al. (1994) detected occurrences of up to two CIRs per solar rotation prior to solar maximum. To incorporate this effect, we introduce a term ρ_γ that would account for the enhanced (short-term) thermospheric density due to periodic CIRs during solar minimum. A comparison between sunspot number, yearly CME, stream CIR interaction, and interplanetary shock rate is shown in Fig. 1. A modified density ρ that includes ρ_γ was used to model the CIR effect,

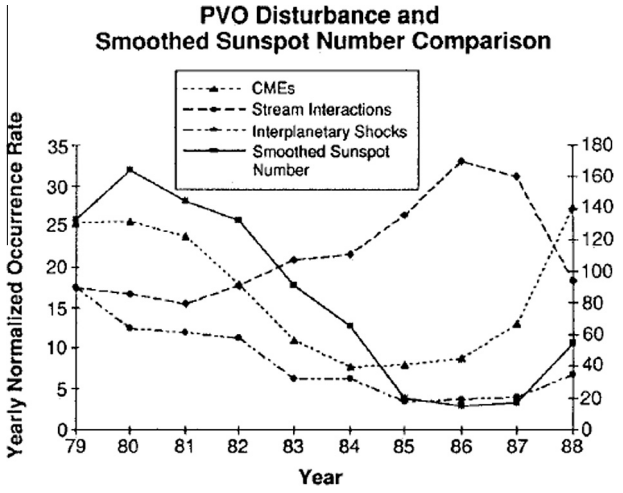

Fig. 1. Comparison between sunspot number (smoothed), CME, CIR, and interplanetary shock rates (Lindsay et al., 1994).

$$\rho = \rho_{bcir} + \rho_{\gamma} \tag{5}$$

where, ρ_{bcir} is the thermospheric density before the CIR and ρ_{γ} is the thermospheric density increase due to CIR-induced effect, modeled as

$$\rho_{\gamma} = (\rho - \rho_{bcir})\alpha \exp[-(\gamma t - 1)^2/2]$$

where, α is the amplitude of density oscillation (ρ increases by a factor of up to 2), γ is the frequency of oscillation ($2\pi/T$), T is the period of oscillation (13.5 days in this study).

5. Results and discussion

5.1. Trends of orbital decay at difference phases of the solar cycle

The model (calculations) of solar cycle (long-term) trends of atmospheric drag due to solar and geomagnetic activity at different phases of a cycle are presented for two maxima (2000–2002 and 2012–2014) and a minimum (2004–2006). Typical range of values of mean altitude, decay rate, thermosphere temperature and density for each satellite in a given regime are provided. The mean annual decay rates of the satellites at different phases were thus estimated.

5.1.1. Solar maximum decay trend

Fig. 2 shows time variations of model satellite's mean altitude, orbit decay rate, thermosphere temperature and density for (a) SAT-BCI and (b) SAT-BCII initially at 450 km in 2000–2002. SAT-BCI (Fig. 2a) experienced a respective decay of 46.13, 49.10 and 47.38 km in 2000, 2001 and 2002, corresponding to a mean decay of 48 ± 2 km per year. The mean orbit decay rate is $47 - 327$ m/day. SAT-BCII (Fig. 2b) respectively decayed by 61.14, 62.23 and 61.19 km (during the same period), corresponding to a mean decay of about 62 ± 1 km per year. The orbit decay rate varied between 55 and 391 m/day. Thermosphere temperature variations during the respective years are $1075 - 1416$, $1021 - 1469$ and $1004 - 1470$ K. Density variations are $2.27 \times 10^{-12} - 7.96 \times 10^{-12}$, $2.06 \times 10^{-12} - 14.70 \times 10^{-12}$ and $1.15 \times 10^{-12} - 8.23 \times 10^{-12}$ kg/m^3 respectively. Extreme values of the computed parameters occurred between July 2001 and early 2002 with up to 30 km decay in 175 days.

5.1.2. Solar minimum decay trend

Fig. 3 shows time variations of model satellite's mean altitude, orbit decay rate, thermosphere temperature and density for (a) SAT-BCI and (b) SAT-BCII initially at 450 km in $2004 - 2006$. SAT-BCI (Fig. 3a) decayed by 13.55, 9.03 and 6.15 km in 2004, 2005 and 2005 respectively, corresponding to an average decay of 10 ± 4 km per year. The mean orbital decay rate is $9 - 92$ m/day. SAT-BCII (Fig. 3b) respectively decayed by 18.77, 12.51 and 8.17 km, corresponding to decay of about 13 ± 6 km per year. The mean variation in orbital decay rate is $10 - 133$ m/day. The respective variations in thermosphere temperature are $834 - 1212$, $790 - 1129$ and $756 - 975$ K. Ranges of density variations are $0.73 \times 10^{-12} - 3.59 \times 10^{-12}$, $0.50 \times 10^{-12} - 1.83 \times 10^{-12}$ and $0.31 \times 10^{-12} - 1.18 \times 10^{-12}$ kg/m^3 respectively. The mean values of computed parameters dropped consecutively in 2004–2006 as solar minimum approached (in 2006). Computation using the CIR effect model produced respective decay of 16.5, 11 and 7.5 km for SAT-BCI and 24.3, 15.8 and 10.7 km for SAT-BCII. The annual mean decay rate is about 12 ± 5 km and 17 ± 8 km per year for SAT-BCI and SAT-BCII respectively. There is an additional $2 - 4$ km decay (per year) from the contribution of assumed periodic occurrence of two CIRs per solar rotation during solar minimum phase.

5.1.3. Emerging solar maximum decay trend

Fig. 4 shows time variations of model satellite's mean altitude, orbit decay rate, thermosphere temperature and density for (a) SAT-BCI and (b) SAT-BCII in 2012–2014. This computation was based on two and a half years archival data (January 2000–June 2014) and 6 months predicted solar radio flux (July–December 2014) and assumed geomagnetic Ap data (NOAA-2). SAT-BCI (Fig. 4a) experienced respective decay of 19.88, 21.17 and 32.44 km in 2012, 2013 and 2014, corresponding to a mean decay of 25 ± 7 km per year. The mean orbit decay rate was $30 - 125$ m/day. SAT-BCII (Fig. 4b) respectively decayed by 24.77, 25.90 and 41.65 km, corresponding to decay of about 31 ± 10 km per year. Mean orbital decay rate varied between 27 and 219 m/day. Thermosphere temperature variations during the respective year are $889 - 1180$, $879 - 1203$ and $959 - 1254$ K. The density variations are $1.48 \times 10^{-12} - 3.03 \times 10^{-12}$, $1.38 \times 10^{-12} - 3.77 \times 10^{-12}$ and $1.62 \times 10^{-12} - 5.51 \times 10^{-12}\, kg/m^3$ respectively. The observed trend in the mean values of computed parameters is a

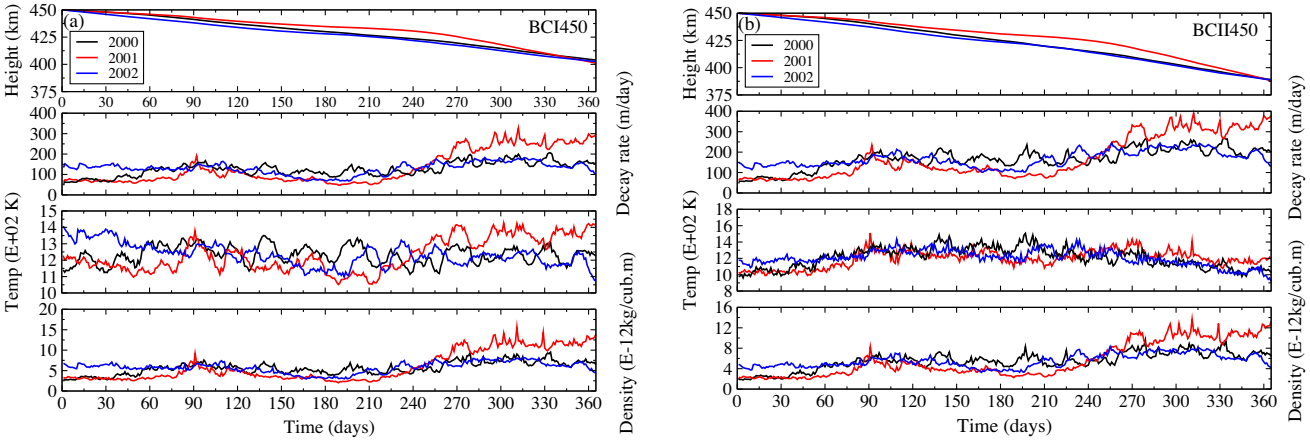

Fig. 2. Time variations of model satellite's mean altitude, orbit decay rate, thermospheric temperature and density in 2000–2002 for (a) SAT-BCI and (b) SAT-BCII.

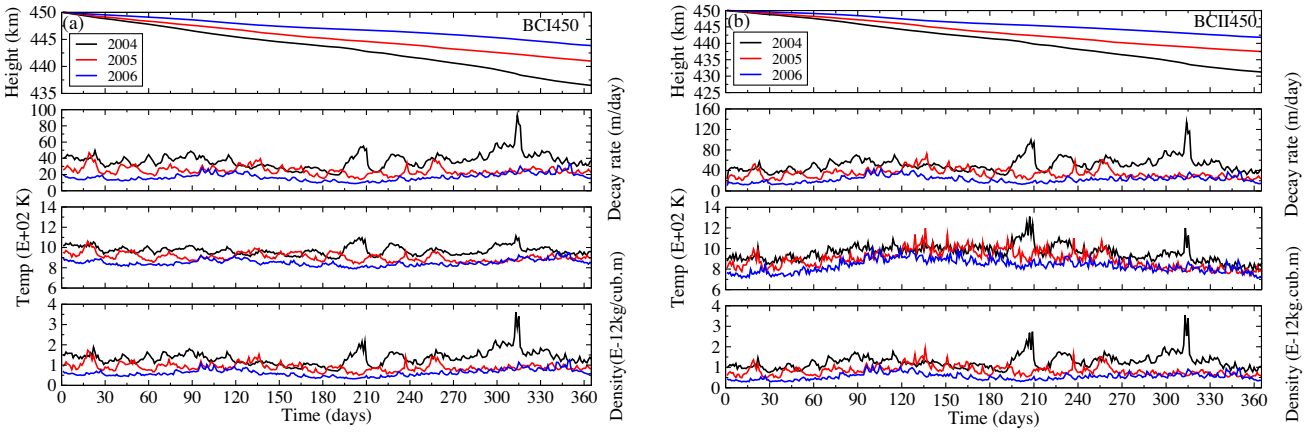

Fig. 3. Time variations of model satellite's mean altitude, orbit decay rate, thermospheric temperature and density in 2004–2006 for (a) SAT-BCI and (b) SAT-BCII.

consecutive increase from 2012 to 2014. The general consensus is that the current solar peak would occur in 2013/2014. Clearly, the annual mean decay rate of both satellites in the current solar peak is half less than the last (2000–2002) peak.

The difference between the area-to-mass ratio of SAT-BCI (0.001) and SAT-BCII (0.00138) is 3.8×10^{-4}. This difference produced decay rate increase of about 13.98, 3.57 and 6.24 km per year in the respective 3 regimes (for SAT-BCII). Summary of the trends of computed parameters for SAT-BCI and SAT-BCII is presented in Table 1.

5.2. Trend of Orbital decay during short-term strong geomagnetic disturbances

Solar data showed significant (high) solar and geomagnetic activity in July 2000. The mean F10.7 and Ap index values during 1st–31st July, 2000 was approximately 200 and 22 respectively; with up to F10.7 = 253 (20th July) and Ap = 152 (15th July). On 14th July, 2000, data showed a record of occurrence of a halo CME (with speed up to 1674 km/s) and associated X class solar flares (X5), followed by solar energetic particle event on 15th July (SOHO; NOAA-3). In Fig. 5, we show plot of values of geomagnetic Ap and disturbance storm time (Dst) index for July 2000. Dst is a measure of geomagnetic activity used to estimate the extent of geomagnetic storms, based on the measure of value of the horizontal component of the Earth's magnetic fields. The strength of the surface magnetic field at low latitudes varies inversely with the energy content of the ring current, which significantly increases during geomagnetic storms (Hamilton et al., 1988). Clearly, there were consequent strong geomagnetic perturbations and storms, associated with preceding solar energetic events - a sudden increase in the number of high speed solar wind particles, fueled by coronal mass ejections and solar flares (Doornbos, 2012), and the increase in solar flux (F10.7) connected with 27-day solar rotation of the active region (Woods et al., 2004; Doornbos, 2012).

In this Section, we investigate the effects of this scenario of periodic (4 weeks) EUV enhancement and the short-

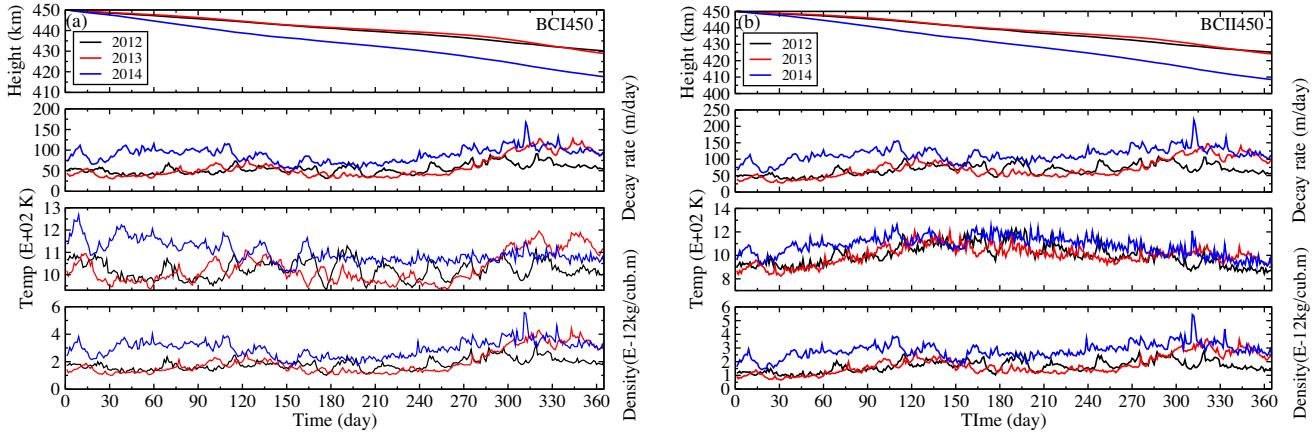

Fig. 4. Time variations of model satellite's altitude, orbit decay rate, thermospheric temperature and density in 2012–2014 for (a) SAT-BCI and (b) SAT-BCII.

Table 1
Trends of time variation of mean altitude, orbit decay rate, thermosphere temperature and density for SAT-BCI and SAT-BCII at different phases of the solar cycle.

Year	Decay (km)		Decay rate (m/day)				Temperature (K)		Density (10^{-12} kg/m^3)	
	BCI	BCII	Low BCI	Low BCII	High BCI	High BCII	Mean Low BCI/BCII	Mean High BCI/BCII	Mean Low BCI/BCII	Mean High BCI/BCII
2000	46.13	61.14	55.00	57.51	205.86	265.28	1075.12	1416.03	2.27	7.96
2001	49.10	62.23	47.25	57.89	327.10	391.31	1021.24	1469.05	2.06	14.70
2002	47.38	61.19	67.68	102.65	182.21	245.62	1004.13	1417.17	3.15	8.23
Mean	47.54	61.52								
2004	13.55	18.77	19.57	23.19	92.85	133.69	834.44	1212.36	0.73	3.59
2005	9.03	12.51	13.91	14.20	46.9	72.33	790.33	1129.29	0.50	1.83
2006	6.15	8.17	9.03	10.33	33.36	43.06	756.22	975.34	0.31	1.18
Mean	9.58	13.15								
2012	19.88	24.77	31.42	35.06	91.15	105.68	889.24	1180.41	1.48	3.03
2013	21.17	25.90	30.51	27.22	127.69	146.87	879.34	1203.29	1.38	3.77
2014	32.44	41.56	53.69	58.94	157.68	219.50	959.18	1254.10	1.62	5.51
Mean	24.50	30.74								

term strong geomagnetic disturbances on the upper atmospheric temperature, density and satellite orbit. Computations were done in three regimes, viz. (1) with actual daily F10.7 and Ap index (raw data) associated with the event ($F_{10.7}, A_p$); (2) mean F10.7 and Ap index during the observed period ($\overline{F_{10.7}, A_p}$), and (3) keeping F10.7 constant (mean value) while Ap (raw) varied accordingly ($\overline{F_{10.7}}, A_p$), in a manner consistent with the disturbances. Fig. 6a and b shows time variations of model satellite's mean altitude, orbit decay rate, thermosphere temperature and density for SAT-BCI and SAT-BCII during 1st–31st July 2000.

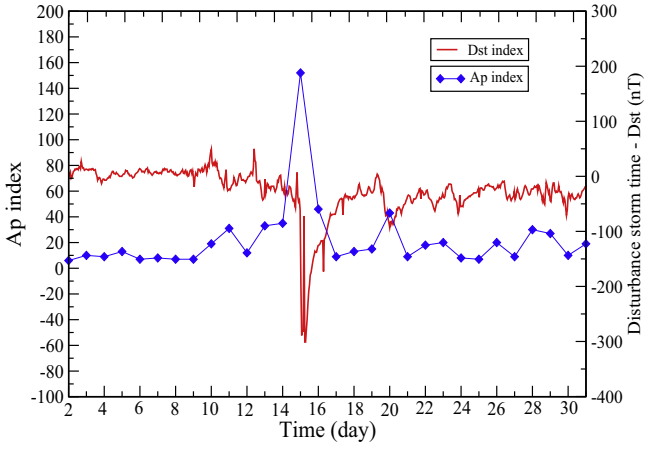

Fig. 5. Ap and Dst index variations during 1st–31st July 2000.

The total decay is about 2.57 km for SAT-BCI and 3.67 km for SAT-BCII. The range of thermospheric temperature and density variations are 1183 – 1407 K and $2.87 \times 10^{-12} - 5.61 \times 10^{-12}$ kg/m^3 respectively. Orbit decay rate for SAT-BCI increased from 63 m/day (1st July) to a peak of 113 m/day on the day of the geomagnetic event (15th July). For SAT-BCII, decay value increased from 91 to 170 m/day. In the third regime (F10.7 constant (red plot)), the decay rate for SAT-BCI increased from a mean value (dotted black line) of 82 m/day to about 111 m/day, and 118 m/day to 166 m/day for SAT-BCII.

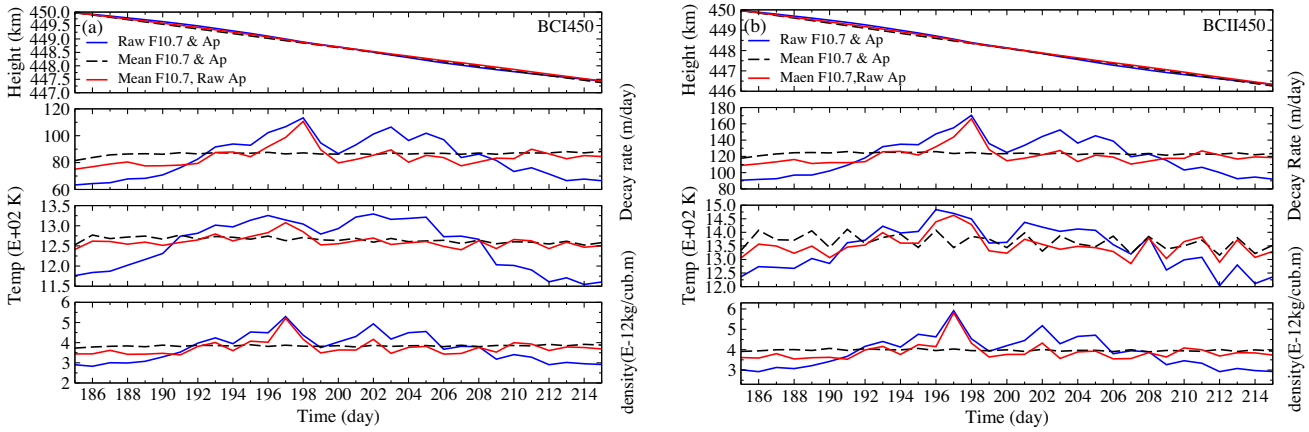

Fig. 6. Time variations of model satellite's mean altitude, orbit decay rate, thermosphere temperature and density for SAT-BCI and SAT-BCII during 1st-31st July 2000.

This corresponds to an additional respective decay of 29 and 48 m/day from short-term geomagnetic disturbances and/or storm-induced thermospheric density perturbations and heating. The summary of variation rates of mean altitude, orbit decay rate, thermospheric temperature and density for SAT-BCI and SAT-BCII during July 2000 is shown in Table 2.

5.3. Model implementation on real satellites' orbit

Xu et al., 2011 investigated effects of periodic variations of thermospheric density on CHAMP (~ 450 km) and GRACE (~ 500 km) satellites orbits. They showed and stated that the orbit of the satellites decayed by 70 and 20 km respectively between 2003 and 2005 due to thermospheric density drag. The Gravity field and steady-state Ocean Circulation Explorer (GOCE) satellite was launched into near-circular orbit with mean altitude 300–250 km in March 2009. GOCE mission ended in October 2013 and re-entered the atmosphere from an approximate height of 224 km on 11 November 2013 (ESA1, 2013; ESA2, 2013). We now implement and/or apply our drag model on CHAMP and GOCE decay scenarios. SAT-BCII has similar ballistic coefficient and orbit as that of CHAMP satellite; $h = 450$ km, $m_s = 522$ kg, $A_s = 0.72$ m^2, $C_d = 2.2$ (Hausleitner et al., 2007; Koppenwallner, 2011). The orbit and ballistic parameters used in this model for GOCE are ~ 268 km (mean height), $m_s = 1100$ kg, $A_s = 1.1$ m^2, $C_d = 3.65$ (Fehringer et al., 2008; Bruinsma and Pilinski, 2011; Koppenwallner, 2011; ESA3, 2013). In Fig. 7, we present the model decay profile of (a) CHAMP for the period 2003–2005 and (b) GOCE during 17th March 2009–21 October 2013 (before re-entry), as a function of actual solar and geomagnetic indices.

CHAMP model result show a decay of about 70.98 km (Fig. 7(a)). There is, however, an approximate 1 km increase in orbital decay when compared with CHAMP's actual decay profile for the period. The peculiarity of GOCE trajectory is its aerodynamic design. The craft was designed to minimize air drag and torque and excludes mechanical disturbances due to the need for low flight and stability. An electric ion thruster at the back of the satellite constantly generate small forces that compensates for any drag in flight. Against this backdrop, we modeled GOCE trajectory with minimal drag force, allowing (conditioned) only 5% of the total drag force experienced by a satellite with similar ballistic coefficient at the injected height. The normal drag force on the satellite was restored (in the simulation) when the spacecraft ran out of fuel (21st October, 2013). The model mean height of GOCE in October 2013 (just before re-entry) is about 224.0487 km (Fig. 7b). The time variations of the satellites' orbit decay rate, thermosphere temperature and density are also consistent with reported values (Koppenwallner, 2011). In Fig. 8, we present the model result of GOCE re-entry evolution between 21st October and 11th November 2013.

Table 2
Trends of time variation of mean altitude, orbit decay rate, thermosphere temperature and density for SAT-BCI and SAT-BCII (initially at $h = 450$ km) during interval of strong geomagnetic perturbations and/or storms in July 2000

	Decay (km)		Decay rate (m/day)				Temperature (K)		Density (10^{-12} kg/m^3)	
	BCI	BCII	Low BCI	Low BCII	High BCI	High BCII	Mean Low BCI/BCII	Mean High BCI/BCII	Mean Low BCI/BCII	Mean High BCI/BCII
$F_{10.7}, A_p$	2.57	3.67	63.36	90.68	113.30	170.39	1183.32	1407.20	2.87	5.61
$\overline{F_{10.7}}, A_p$	2.63	3.74	81.53	117.64	88.25	124.77	1284.41	1344.14	3.82	3.99
$\overline{F_{10.7}}, A_p$	2.56	3.66	75.11	108.84	110.65	166.15	1265.09	1386.40	3.50	5.52

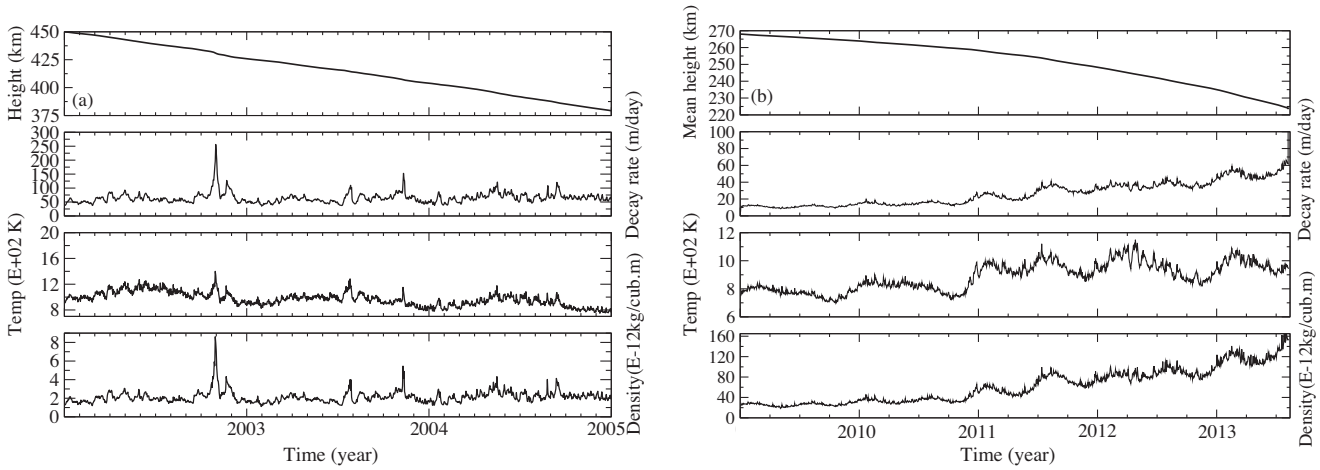

Fig. 7. Model decay profile of (a) CHAMP satellite during 2003–2005 (b) GOCE satellite during 2009–2013.

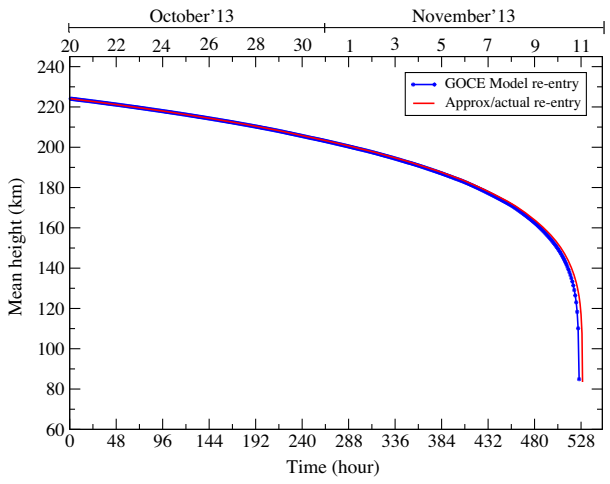

Fig. 8. Model re-entry evolution of GOCE satellite during 21st October–11 November 2013.

The model GOCE re-entry (blue curve) is compared with the approximate/actual re-entry (red curve) evolution. Model re-entry occurred about 5 h (10/11/2013, 20:00 CET) before the actual/reported re-entry (11/11/2013, 01:00 CET). The deviations in our model results are ~ 1 km for CHAMP decay profile and ~ 5 h for GOCE re-entry evolution. However, our computed/modeled values compare well with the real-time decay and/or re-entry evolution of these real satellites. In view of the computational inadequacies, this work/model is being improved for better accuracy and expanded to include application on more LEO satellite under varying space environmental conditions.

6. Conclusion

The model of atmospheric drag on the orbit of two hypothetical LEO satellites is presented in this paper. We model and compared how satellites of different ballistic coefficients respond to the effect. We investigated consequences of solar cycle variations on the orbit of the satellites and during interval of strong geomagnetic activity, mainly results of solar forcing induced perturbations and heating of thermospheric density; driven by solar energetic events. We show dependence of orbital decay rate on the severity of both solar cycle and phase. The mean yearly decay rate during the last solar max (2000–2002) was almost twice that of current phase (2012–2014): [48 ± 2, 62 ± 1 km/year] and [25 ± 7, 31 ± 10 km/year] respectively for the model Satellites (SAT-BCI and SAT-BCII). However, depending on ballistic coefficient and nature of a solar cycle phase, a typical LEO satellite initially at $h = 450$ km could experience a decay rate of up to 41 ± 19 km per year (~ 3 km/month) during solar maximum and 11 ± 6 km per year (~ 1 km/month) during the solar minimum. Dominant CIR-induced effects during solar minimum phase could result to additional decay rate of up to 3 km/year. We showed that intervals of strong density perturbations and additional heating due to geomagnetic activity and/or storms can result in an additional 60% decay in each event. This impact could vary depending on the severity and duration of the event. In the literature similar drag effects are computed often taking average behavior. We show in our simulations the importance of taking the sequence of events into account. Two events E_1 and E_2 may produce different impacts if they occurred in a reversed sequence. Extending this logic to solar cycles, the results of a launch in a solar minimum would be different from that in a solar maximum even if both satellites survives for, say a full cycle. This is due to strong non-linearity in drag effects. This aspect and an extended application of this model to more LEO satellites and solar cycles would be reported in another paper.

Acknowledgment

VUJN acknowledges TWAS/ICTP, Trieste, Italy and S.N. Bose National Centre for TWAS-Bose research fellowship. Authors thank reviewers for their resourceful comments and suggestions.

References

Alfonsi, L., Kavanagh, Andrew J., Amata, Ermanno, Cilliers, Pierre, Correia, Emilia, Freeman, Mervyn, Kauristie, Kirsti, Liu, Ruiyuan, Mitchell, Cathryn N., Luntama, Juha-Pekka, Zherebtsov, G.A., 2008. Probing the high latitude ionosphere from ground-based observations: the state of current knowledge and capabilities during IPY (2007–2009). J. Atmos. Solar-Terr. Phys. 70, 2293–2308.

Borovsky, J.E., Denton, M.H., 2006. Differences between CME-driven storms and CIR-driven storms. J. Geophys. Res. 111, A07S08. http://dx.doi.org/10.1029/2005JA011447.

Bounsanto, M.J., 1999. Ionospheric storms a review. Space Sci. Rev. 88, 563601.

Bowman, B.R., Kent Tobiska, W., Kendra, Michael J., 2008. The thermospheric semiannual density response to solar EUV heating. J. Atmos. Solar-Terr. Phys. 70 (11–12), 14821496. http://dx.doi.org/10.1016/j.jastp.2008.04.020.

Bruinsma, S., Pilinski, M., 2011. Drag coefficients. NADIR workshop – October 25–26.

Bruinsma, S., Thuillier, G., Barlier, F., 2003. The DTM-2000 empirical thermosphere model with new data assimilation and constraints at lower boundary: accuracy and properties. J. Atmos. Solar-Terr. Phys. 65 (9), 1053–1070.

Burns, A.G., Solomon, S.C., Qian, L., Wang, W., Emery, B.A., Wiltberger, M., Weimer, D.R., 2012. The effects of Corotating interaction region/High speed stream storms on the thermosphere and ionosphere during the last solar minimum. J. Atmos. Solar-Terr. Phys. 83, 79–87.

Chen, G., Jiyao, Xu., Wang, Wenbin, Lei, Jiuhou, Burns, Alan G., 2012. A comparison of the effects of CIR- and CME-induced geomagnetic activity on thermospheric densities and spacecraft orbits: case studies. J. Geophys. Res. 117, A08315. http://dx.doi.org/10.1029/2012JA017782.

Chobotov, V.A., 2002. Orbital Mechanics, third ed., AIAA Education Series. American Institute of Aeronautics Inc, Virginia, 629.4113, pp. 193–213.

Deng, Y., Huang, Y., Solomon, S., Qian, L., Knipp, D., Weimer, D.R., Wang, J.S., 2012. Anomalously low geomagnetic energy inputs during 2008 solar minimum. J. Geophys. Res. 117, A09307. http://dx.doi.org/10.1029/2012JA018039.

Doornbos, E., 2012. Density and Wind Determination from Satellite Dynamics. Thermospheric. Springer-Verlag, Berlin Heidelberg. http://dx.doi.org/10.1007/978-3-642-25129-02, Springer Theses.

Doornbos, E., Klinkrad, H., 2006. Modelling of space weather effects on satellite drag. Adv. Space Res. 37, 12291239.

Emmert, J.T., Picone, M., 2010. Climatology of globally averaged thermospheric mass density. J. Geophys. Res. 115, A09326.

ESA1, 2013. GOCE Completes its Mission. European Space Agency.

ESA2, 2013. GOCE Gives in to Gravity. European Space Agency.

ESA3, 2013. GOCE Satellite. European Space Agency.

Fehringer, M., Andre, Gerard, Lamarre, Daniel, Maeusli, Damien, 2008. GOCE: a jewel in ESA's crown. ESA Bull. 133, 14–23.

Forbes, J., Bruinsma, S.L., Zhang, X., Oberheide, J., 2009. Surface-exosphere coupling due to thermal tides. Geophys. Res. Lett. 36 (15), L15812.

Gopalswamy, N., 2009. Coronal mass ejections and space weather. In: Climate and Weather of the Sun System (CAWSES). TERRAPUB, Tokyo, pp. p 77–118.

Gosling, J.T., Pizzo, V.J., 1999. Formation and evolution of corotating interaction regions and their three dimensional structure. Space Sci. Rev. 89, 2152.

Hagan, M., Forbes, J., 2002. Migrating and non-migrating diurnal tides in the middle and upper atmosphere excited by tropospheric latent heat release. J. Geophys. Res. 107 (D24), 4754.

Hausleitner, W., Krauss, S., Stangl, G., Weingrill, J., Lichtenegger, H.I.M., Lammer, H., Khodachenko, M.L., 2007. Response of LEO satellite drag parameters to anomalies in the upper atmosphere during extreme solar events. In: Physics of Auroral Phenomena, Proc. XXX Annual Seminar, Kola Science Centre, Russian Academy of Science, Apatity, pp. 158–162.

IRS Radio, 1999. & Space Services, Satellite Orbital Decay Calculations. Australian Space Weather Agency, Sydney.

Kim, K.H., Moon, Y.J., Cho, K.S., Kim, H.D., Park, J.-Y., 2006. Atmospheric drag effects on the KOMPSAT-1 satellite during geomagnetic superstorms. E-letter Earth Planets Space 58, e25–e28.

Klenzing, J., Burrell, A.G., Heelis, R.A., Huba, J.D., Pfaff, R., Simes, F., 2013. Exploring the role of ionospheric drivers during the extreme solar minimum of 2008. Ann. Geophys. 31, 21472156. http://dx.doi.org/10.5194/angeo-31-2147-2013.

Klinkrad, H., 1996. On the use of atmosphere models in re-entry predictions. In: Environment Modelling for Space-based Applications, Symposium Proceedings (ESA SP-392). ESTEC Noordwijk, pp. 287–298.

Koppenwallner, G., 2011. Satellite aerodynamics and determination of thermospheric density and wind. In: AIP Conf. Proc. 1333, Pacific Grove, California, p. 1307.

Kutiev, I., Tsagouri, Ioanna, Perrone, Loredana, Pancheva, Dora, Mukhtarov, Plamen, Mikhailov, Andrei, Lastovicka, Jan, Jakowski, Norbert, Buresova, Dalia, Blanch, Estefania, Andonov, Borislav, Altadill, David, Magdaleno, Sergio, Parisi, Mario, Torta, Joan Miquel, 2013. Solar activity impact on the Earths upper atmosphere. J. Space Weather Space Clim. 3, A06. http://dx.doi.org/10.1051/swsc/2013028.

Kwak, Y.-S., Kim, K.-H., Deng, Y., Forbes, J.M., 2011. Response of thermosphere density to changes in interplanetary magnetic field sector polarity. J. Geophys. Res. 116, A11316.

Lei, J., Thayer, J.P., Forbes, J.M., Sutton, E.K., Nerem, R.S., Temmer, M., Veronig, A.M., 2008. Global thermospheric density variations caused by high-speed solar wind streams during the declining phase of solar cycle 23. J. Geophys. Res. 113 (A11). http://dx.doi.org/10.1029/2008JA013433.

Lei, J., Guangming Chen, Jiyao Xu, Xiankang Dou, 2013. Impact of Solar Forcing on Thermospheric Densities and Spacecraft Orbits from CHAMP and GRACE, Intech open science, doi: 10.5772/56599.

Leonard, J.M., Forbes, J., Born, G.H., 2012. Impact of tidal density variability on orbital and reentry predictions. Space Weather 10, S12003. http://dx.doi.org/10.1029/2012SW000842.

Lindsay, G.M., Russell, C.T., Luhmann, J.G., 1994. On the sources of interplanetary shocks at 0.72 AU. J. Geophys. Res. 99, 11–17.

Liu, J., Liu, Libo, Zhao, Biqiang, Thayer, Jeffrey P., Lei, Jiuhou, McPherron, Robert L., 2012. Superposed epoch analyses of thermospheric response to CIRs: solar cycle and seasonal dependencies. J. Geophys. Res. 117, A00L10. http://dx.doi.org/10.1029/2011JA017315.

Liu, H., Hirano, T., Watanabe, S., 2013. Empirical model of the thermospheric mass density based on CHAMP satellite observation. J. Geophys. Res. Space Phys. 118, 843848. http://dx.doi.org/10.1002/jgra.50144.

NOAA-1, Solar Particle and Geomagnetic Indices. <www.swpc.noaa.gov/ftpmenu/indices/oldindices.html> (Retrieved March 2011).

NOAA-2, Predicted Sunspot Number And Radio Flux Values With Expected Ranges. <www.swpc.noaa.gov/ftpdir/weekly/Predict.txt> (Retrieved March 2011).

NOAA, 2006. Satellites and space weather. <www.swpc.noaa.gov/info/satellites.html>.

NOAA-3, Solar Proton Events Affecting the Earth Environment. NOAA Space Weather Prediction Center. <www.swpc.noaa.gov/ftpdir/indices/SPE.txt/> (Retrieved March 2011).

Nwankwo, V.U.J., Chakrabarti, K.S., 2014. Theoretical modeling of drag force impact on a model international space station (ISS) during variation of solar activity. Trans. JSASS Aerosp. Technol. Jpn. 12, 47–53.

Nwankwo, V.U.J., Chakrabarti, S.K., 2015. Analysis of planetary and solar induced perturbations on trans-Martian trajectory of Mars missions before and after Mars orbit insertion. Indian J. Phys.

Oberheide, J., Forbes, J., Husler, K., Wu, Q., Bruinsma, S.L., 2009. Tropospheric tides from 80–400 km: propagation, interannual variability and solar cycle effects. J. Geophys. Res. 114, D00105.

Pardini, C., Tobiska, K., Luciano, A., 2004. Analysis of the orbital decay of spherical satellites using different solar flux proxies and atmospheric density models. Adv. Space Res. 37 (2), 392–400.

Picone, J.M., Hedin, A.E., Drob, D.P., Aikin, A.C., 2002. NRLMSISE-00 empirical model of the atmosphere: Statistical comparisons and scientific issues. J. Geophys. Res. 107 (A12), 1468.

Policastri, L.A., Joseph, M., Simons, 2003. Implementing the MSIS atmospheric density model in OCEAN, AAS 03-166.

Rhoden, E.A., Forbes, J.M., Marcos, F.A., 2000. The influence of geomagnetic and solar variabilities on lower thermosphere density. J. Atmos. Solar-Terr. Phys. 62, 999–1013.

Richardson, I.G., Cliver, E.W., Cane, H.V., 2001. Sources of geomagnetic storms for solar minimum and maximum conditions during 19722000. Geophys. Res. Lett. 28 (13), 25692572.

SOHO/LASCO, SOHO LASCO CME CATALOG. cdaw.gsfc.nasa.gov/CMElist (Retrieved March 2011).

Solomon, S.C., Burns, Alan G., Emery, Barbara A., Mlynczak, Martin G., Qian, Liying, Wang, Wenbin, Weimer, Daniel R., Wiltberger, Michael, 2012. Modeling studies of the impact of high-speed streams and co-rotating interaction regions on the thermosphere-ionosphere. J. Geophys. Res. 117, A00L11.

Storz, Mark F., Bowman, Bruce R., Branson, Major James I., Casali, Stephen J., Kent Tobiska, W., 2005. High accuracy satellite drag model (HASDM). Adv. Space Res. 36, 24972505.

Storz, M.F., Bruce, R., Bowman, Major James, Branson, I., Casali, Stephen J., Kent Tobiska, W., 2005. High accuracy satellite drag model (HASDM). Adv. Space Res. 36, 24972505.

Sutton, E.K., Forbes, J.M., Nerem, R.S., 2005. Global thermospheric neutral density and wind response to the severe 2003 geomagnetic storms from CHAMP accelerometer data. J. Geophys. Res. 110 (A9).

Tsurutani, B.T., Gonzalez, Alicia L.C., Gonzalez, Walter D., Guarnieri, Fernando L., Gopalswamy, Nat, Grande, Manuel, Kamide, Yohsuke, Kasahara, Yoshiya, Lu, Gang, Mann, Ian, McPherron, Robert, Soraas, Finn, Vasyliunas, Vytenis, 2006. Corotating solar wind streams and recurrent geomagnetic activity: a review. J. Geophys. Res.: Space Phys. 111, A07S01. http://dx.doi.org/10.1029/2005JA011273.

Walterscheid, R.L., 1989. Solar cycle effects on the upper atmosphere – implications for satellite drag. J. Spacecraft Rockets 26 (6), 439–444. http://dx.doi.org/10.2514/3.26089.

Weigel, R.S., 2010. Solar wind density influence on geomagnetic storm intensity. J. Geophys. Res. 115, A09201. http://dx.doi.org/10.1029/2009JA015062.

Weigel, R.S., Baker, Daniel N., Joshua Rigler, E., Vassiliadis, Dimitris, 2004. Predictability of large geomagnetic disturbances based on solar wind conditions. IEEE Trans. Plasma Sci. 32 (4), 1506–1510.

Wertz, J., Larson, W.J., 1999. Space Mission Analysis and Design, third ed. Kluwer Academy, El Segundo, Calif, pp 145.

Woods, T., Loren W. Acton, Scott Bailey, Frank Eparvierl, Howard Garcia, Darrell Judges, Judith Lean, John T. Mariska, Don McMullin, Gerhard Schmidtke, Stanley C. Solomon, Kent Tobiska, W., Harry P. Warrenlo, Rodney Viereck, 2004. Solar extreme ultraviolet and x-ray irradiance variations. Solar variability and its effects on climate, Geophysical Monograph 141, American Geophysical Union, doi:10.1029/141GM11.

Xu, J., Wang, W., Lei, J., Sutton, E.K., Chen, G., 2011. The effect of periodic variations of thermospheric density on CHAMP and GRACE orbits. J. Geophys. Res. (Space Phys.) 116 (A15), 2315. http://dx.doi.org/10.1029/2010JA015995.

Zhang, X., Forbes, J., Hagan, 2010. Longitudinal variation of tides in the MLT region: 1. Tides driven by tropospheric net radiative heating. J. Geophys. Res. 115, A06316.

Further reading

Bowman, B., Pilinski, M., 2011. Drag coefficients. NADIR workshop – October 25–26.